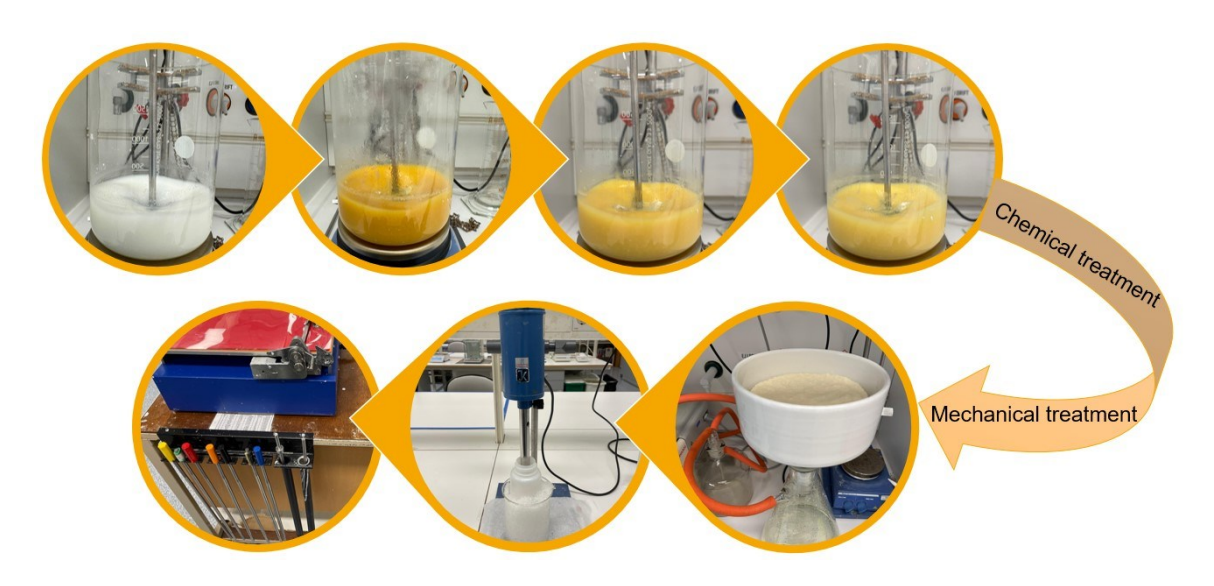
Hardwood-derived Cellulose Nanofibrils and Micro-Fibrillated Cellulose *via* Fenton Pretreatment: Issues of Fiber Fragmentation and Coating Performance

Morassa Raouf ,* Björn Sjöstrand , and Agne Swerin

* Corresponding author: Morassa.raouf@kau.se

DOI: 10.15376/biores.21.1.397-419

GRAPHICAL ABSTRACT



Hardwood-derived Cellulose Nanofibrils and Micro-Fibrillated Cellulose *via* Fenton Pretreatment: Issues of Fiber Fragmentation and Coating Performance

Morassa Raouf ,* Björn Sjöstrand , and Agne Swerin

A novel cellulose nano material was prepared through a controlled Fenton oxidation process utilizing hydrogen peroxide and ferrous ions. The reaction parameters enabled ferrous-catalyzed oxidation, which combined with mechanical treatment resulted in an effective fibrillation of cellulose fibers. Optical microscopy images provided a visual comparison of fiber morphology between untreated hardwood pulp and Fenton-treated samples, clearly illustrating the fibrillation effect. The samples were evaluated for fiber drainage behavior, and conclusions about accessibility and the extent of fibrillation were made. Measurements of the surface charge of the samples revealed an increase in negative charges originating from added carboxyl groups, which is essential for the dispersing and stabilization of cellulose nano fibrils and micro-fibrillated cellulose (CNF/MFC). Fourier-transform infrared spectroscopy (FTIR) confirmed the introduction of the carboxyl groups due to the Fenton treatment. The CNF/MFC material was used as paper coatings, without adding additional materials. The coated samples underwent analyses of permeability and roughness, revealing possibilities for enhancements in barrier properties and hydrophobicity. The results emphasize the ability of Fenton oxidation in generating high-quality small scale cellulosic materials with customized functionalities, underscoring their potential application in advanced coating technologies and sustainable material innovation.

DOI: 10.15376/biores.21.1.397-419

Keywords: Fenton oxidation; Cellulose nano fibril (CNF); Micro-fibrillated cellulose (MFC); Hardwood; Barrier; Coating

Contact information: Pro2BE academic environment in Processes and products for a circular biobased economy at the Department of Engineering and Chemical Sciences, Karlstad University, Sweden; *Corresponding author: Morassa.raouf@kau.se

INTRODUCTION

Cellulose-based materials are derived from the most abundant renewable polymer on Earth and offer a wide range of applications due to their biodegradability, cost-effectiveness, and versatile functionality. These materials have attracted significant attention across multiple sectors, particularly in packaging, coatings, and sustainable product design, owing to their unique properties and modifiability (Sulaiman *et al.* 2015; Petroudy *et al.* 2021).

Although cellulose-based materials have long been used in industrial scale processes, especially in traditional sectors including pulp and paper and wood processing, new modifications aimed at replacing fossil-based plastics and enabling advanced functionalities bring new challenges. Among these, cellulose nanofibrils (CNF) and microfibrillated cellulose (MFC) show mechanical, physical, and functional characteristics that

allow for more advanced applications (Nagarajan *et al.* 2019). However, their industrial production still faces significant obstacles, particularly in scaling up while ensuring consistent quality, due largely to energy-intensive processes such as dewatering and drying (Boufi *et al.* 2016).

The conversion of cellulose fibers into CNF and MFC is driven by the need to leverage the unique properties that emerge at the nano- and microscale. Recent studies have introduced innovative methods for producing high-quality CNF and MFC suitable for coating and other functional uses. For example, Li *et al.* (2014) utilized a hydrated deep eutectic solvent (choline chloride, oxalic acid, water) to carboxylate cellulose, yielding ultrafine CNFs with high mass yield and process recyclability. In another approach, Abraham *et al.* (2013) demonstrated that high doses of endoglucanase can produce CNF with up to 23% nano fibrillation yield and high cationic demand. They also developed a machine-learning model to predict sugar release, supporting real-time process control. Altogether, green solvents, continuous milling, flotation, and enzyme-assisted fibrillation are among the strategies that have shown improved yields or reduced energy use, advancing the scalability of CNF/MFC production (Liu *et al.* 2017; Sulaiman *et al.* 2015).

Despite these developments, dewatering and drying remain major technical challenges in the manufacture of CNF and MFC. Since nanocellulose is typically generated as a dilute suspension (often below 1% solids), the transportation and post-processing steps are costly. Additionally, converting this into dry powder form is difficult due to high viscosity and gel formation at low solid content. Reviews have emphasized that removing water without damaging the nanoscale structure remains a substantial bottleneck (Pouran et al. 2015; Bahrami et al. 2018). While some laboratory-scale drying methods such as freeze-drying, centrifugation, and dewatering process show promise, but they are often limited by high energy demands or adverse impacts on material properties.

Consequently, many CNF/MFC production approaches continue to rely on slurry forms, with direct formulation into coatings or composites. Novel methods that allow for higher solid contents—such as solvent-assisted fibrillation or integrated dewatering units—are under active investigation (Liu *et al.* 2017).

CNFs exhibit superior mechanical strength, water-holding capacity, improved barrier properties, and higher surface charge in comparison to untreated pulp fibers. These attributes make them highly suitable for applications in sustainable packaging, functional coatings, composite materials, filtration membranes, biomedical products, and as reinforcing agents in papermaking (Li *et al.* 2022; Menezes *et al.* 2021). Furthermore, their colloidal stability and tunable surface chemistry contribute to better compatibility with additives and other materials (Pouran *et al.* 2015; Paniz *et al.* 2020).

Particularly, CNFs and MFCs derived from hardwood pulp have gained attention due to their renewability, biodegradability, high specific surface area, and excellent mechanical properties. These materials are ideal for new developments in renewable product formulations. The preparation of CNF/MFC from hardwood pulp involves multiple techniques and yields various functional benefits (Li *et al.* 2022). Other methods, such as enzymatic, chemical, and mechanical treatments, generate nano-porous structures suitable for advanced applications due to their high thermal resistance and electrolyte uptake (Nagarajan *et al.* 2019; Potulski *et al.* 2020).

Earlier work by Hellström (2015) provides an important foundation for this study, demonstrating the potential of Fenton pre-treatment to improve the production and performance of micro fibrillated cellulose (MFC). In this work, bleached birch kraft pulp was treated with acidic hydrogen peroxide in the presence of ferrous ions, which reduced

the degree of polymerization while increasing carboxyl and carbonyl group content along the cellulose chain. These chemical modifications made subsequent mechanical fibrillation easier and more energy-efficient, producing MFC with a higher proportion of smaller size of fibrils. When evaluated in paperboard test sheets, Fenton-pre-treated MFC showed significantly enhanced strength performance, achieving approximately 50% improvement in z-directional strength and notable increases in tensile stiffness and tensile index compared to sheets without MFC addition. The study also compared Fenton pre-treatment with enzymatic approaches, revealing that the former offered greater surface functionality and better reinforcement properties for industrial applications.

The Fenton oxidation process—traditionally applied in wastewater treatment—has been adapted here for nanocellulose fabrication. It involves hydrogen peroxide (H₂O₂) and ferrous ions (Fe²⁺), generating hydroxyl radicals that selectively oxidize cellulose. This leads to the introduction of carboxyl and carbonyl functional groups on the fiber surface, which improve both hydrophilicity and chemical reactivity (Ruelas *et al.* 2023; Li *et al.* 2018). Such modification aids in breaking down papermaking fibers into nano- and microsized fibrils and enhances their dispersion and bonding potential for applications such as barrier coatings (Bautista *et al.* 2008; Boufi *et al.* 2016).

Fenton oxidation is an efficient pretreatment for producing CNF compared with TEMPO-mediated oxidation. It is cost-effective, operates under mild conditions, and efficiently promotes fiber fibrillation. Furthermore, the Fenton treatment produces MFC with a higher proportion of small, well-fibrillated particles, as demonstrated by fractionation and scanning electron microscopy, outperforming enzymatic and acid pretreatment methods in generating uniform nanofibrils (Hellström *et al.* 2015). In contrast, the TEMPO-mediated oxidation is highly sensitive to parameters such as pH, temperature, and reaction time, and it requires careful control of the oxidant-to-cellulose ratio to avoid over-oxidation or fiber degradation. These strict operational requirements, along with the use of costly catalysts and strict reaction conditions, limit its scalability and practical application compared with the more robust Fenton process (Gamelas *et al.* 2015; Hellström *et al.* 2015).

By varying the Fenton process parameters—including the concentration of H₂O₂, Fe²⁺, reaction pH, and treatment duration—one can tailor the resulting CNF/MFC characteristics. This flexibility enables the design of sustainable, high-performance nanocellulose materials for industrial use (Hellström *et al.* 2015; Bautista *et al.* 2008).

The aim of this study was to combine Fenton oxidation with mechanical dispersion to efficiently produce CNF/MFC from hardwood pulp and to evaluate their application in paper coatings, focusing on improvements in air permeability and water resistance. This research addresses several key questions: How does Fenton oxidation influence the chemical and morphological properties of hardwood pulp fibers? To what extent does subsequent mechanical dispersion enhance fibrillation and surface area? How do these treatments affect the air and water barrier properties of CNF/MFC coatings? What are the optimal conditions, such as dispersing duration and coat weight, for achieving significant performance improvements in paper coatings? By investigating these questions, the study sought to elucidate the relationship between chemical pretreatment, mechanical processing, and functional properties.

EXPERIMENTAL

Materials

Never dried fully bleached chemical kraft pulp fibers of birch (Betula pendula/pubescens) from Gruvön Mill (Billerud AB, Sweden) were used as the raw material. Hydrogen peroxide (H₂O₂, 30 wt%) and ferrous sulfate heptahydrate (FeSO₄·7H₂O₅, 99%) were obtained from Sigma-Aldrich and used without further purification. Throughout this study, the original pulp was treated chemically and mechanically, with pulp samples taken away and analyzed at each step, in order to follow the development of the treatments.

Chemical Treatment

A 10 wt.% suspension of hardwood pulp was prepared in deionized water and stirred using a propeller mixer. The pH was adjusted to approximately pH 3, using sulfuric acid. Then, 1.5 g ferrous sulfate was added and stirred at room temperature. The suspension was vacuum filtered on Büchner funnel using a polyester mesh filter (SEFAR PETEX 07-120/34 with a 120-micron mesh opening and 34% open area, Switzerland). Then, 10 mg/mL hydrogen peroxide was added and stirred at 45 °C for 5 h. Eqs. 1 to 4 are showing the reactions happening during the chemical treatment.

$$FeSO_{4} * 7H_{2}O \rightarrow Fe^{2+} + SO_{4}^{2-} + 7H_{2}O$$

$$Fe^{2+} + H_{2}O_{2} \rightarrow Fe^{3+} + \bullet OH + OH^{-}$$

$$Fe^{3+} + H_{2}O_{2} \rightarrow Fe^{2+} + \bullet OOH + H^{+}$$
(3)

$$Fe^{2+} + H_2O_2 \rightarrow Fe^{3+} + \bullet OH + OH^-$$
 (2)

$$Fe^{3+} + H_2O_2 \rightarrow Fe^{2+} + \bullet OOH + H^+$$
 (3)

$$FeSO_4 + H_2O_2 + H_2SO_4 \rightarrow Fe^{3+} + OH^{\bullet} + OH^{-} + SO_4^{2-}$$
 (4)

A significant color change of the suspension was observed as the reaction proceeded, where it started as a white mixture before H₂O₂ addition, turning dark yellow early after, and slowly moving towards lighter yellow (Fig. 1).

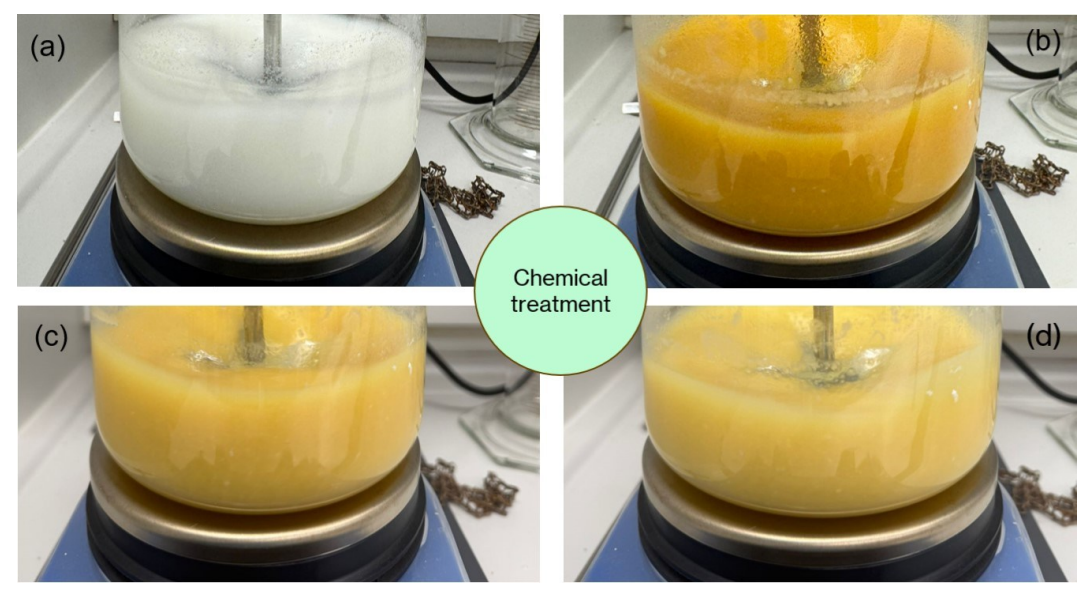


Fig. 1. Chemical treatment steps applied to the hardwood pulp: (a) hardwood pulp mixed with FeSO₄ and deionized water at room temperature, (b) pulp mixture after addition of H₂O₂ and heating at 45 °C for 1 h, (c) pulp mixture after 3 h at 45 °C, and (d) pulp mixture after 5 h at 45 °C

The suspension was considered ready when the color of the suspension was stabilized. The final suspension was washed with deionized water repeatedly until the conductivity of the filtrate reached less than 5 μ S/cm, measured with a conductivity meter. A picture series of the Fenton oxidation procedure applied to the hardwood pulp is presented in Fig. 1. The reactions involved in the Fenton pretreatment are shown below:

Mechanical Treatment

Following the Fenton oxidation treatment, a mechanical dispersing step was applied using an ultra-turrax disperser (IKA-Werke GmbH & Co. KG, Staufen, Germany) to enhance the fibrillation of oxidized cellulose fibers. This step subjects the chemically modified fibers to controlled mechanical shear, breaking down fibers into micro and nanofibrils. To evaluate the effect of mechanical input on fibrillation, the disperser (operating at 10,000 rpm) was operated for varying durations: 15, 30, 60, and 90 min. The ultra-turrax disperser is a high-shear rotor–stator device that generates intense and uniform shear forces, effectively promoting fibrillation. Its controlled shear environment allows precise adjustment of processing in different time duration (15 to 90 min) and intensity, making it suitable for the mechanical treatment to produce CNF/MFC. The overall schematic of Fenton oxidation process (including chemical and mechanical treatments) for producing CNF/MFC is shown in Fig. 2.

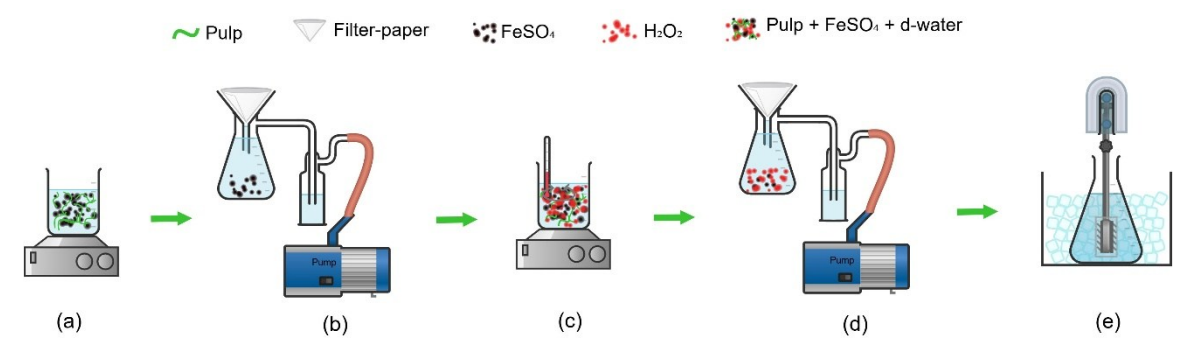


Fig. 2. Fenton oxidation process (chemical and mechanical treatments) schematic: (a) Hardwood pulp mixing with FeSO₄ and deionized water at room temperature for 1 hour, (b) Filtering the excess of FeSO4 by Vacuum pump, (c) Adding H_2O_2 to the mixture (a) at 45 °C and stirring for 5 hours, (d) Filtering the suspension until the conductivity value reaches to less than 5 μ S/cm by vacuum pump, (e) Dispersing the suspension with ultra-turrax disperser for 15 to 90 minute in an ice-bath

Coating Process

The CNF/MFC suspensions were utilized for coating process by using a laboratory coating bench (K Control Coater, RK Print-Coat Instruments Ltd., Royston, UK) equipped with different adjustable rod applicators to control the coat weight. CNF/MFC coatings were applied onto DCP A4 paper from Claire Fontaine (250±0.2 g/m², Whiteness CIE170, Double-sided printing, ÉtivalClaire Fontaine, France), this base paper was chosen due to it low variation in basis weight. The basis weight was controlled by measuring ten separate sheets and the 95 % confidence interval was calculated to 0.2 g/m². The coating suspension concentration, the coating rod speed, and the added coating volume were all adjusted in order to create uniform coatings between 1.5 and 3.7 g/m² and to ensure a smooth and continuous application. The rod was locked and not rotating during the coating process. Solids contents, rod speeds and coating volumes corresponding to approximate achieved coat weights are shown in Table 1.

Rod speed (cm/s)	Coating concentration (wt%)	Coating volume (mL)	Approximate achieved coat weight (g/m²)
7.5	1.0	4.0	1.5
5.5	1.5	3.5	2.0
5.5	2.0	3.3	2.5
5.5	2.5	3.2	3.0
3.5	2.5	3.7	3.5

Table 1. Coating Settings for Bench Coating of CNF

Following coating, sheets were dried and conditioned restrained by elongated weights on all four sides of the papers at 105 °C in an oven for 15 min and then conditioned in a controlled climate of 23 °C and 50% relative humidity (ISO 187:2022) and kept for 24 hours. The coated papers were cut according to the coated section and then weighed. The coat weights were verified gravimetrically. The uncoated DCP paper served as the reference (REF) for comparison of surface, optical, and barrier properties. The CNF/MFC coating steps are shown in Fig. 3.

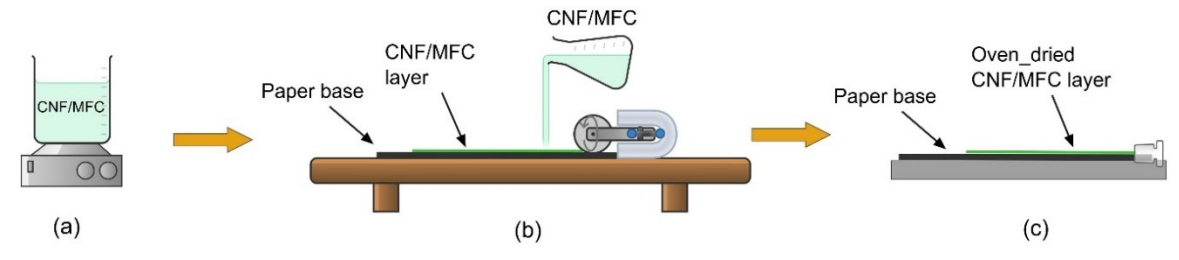


Fig. 3. Stepwise process schematic for CNF/MFC coating: (a) Stirring CNF/MFC suspension for 15 min at room temperature, (b) coating a layer of CNF/MFC on paper-base by using rotary-rod bench, (c) keeping CNF/MFC coated sheets in the oven for 15 min before transferring to the climate room for 24 hours

Fourier-Transform Infrared Spectroscopy

Fourier-transform infrared (FTIR) spectroscopy was employed to characterize the chemical composition changes in the original pulp (OP) and CNF/MFC samples following varying mechanical dispersing times (0 and 90 min). The FTIR spectra were recorded in accordance with ISO 20579-3 (2021) using an Agilent Cary 630 ATR-FTIR spectrometer (Agilent Technologies, Santa Clara, California, USA) for the samples: OP0, OP90, CNF/MFC0, and CNF/MFC90. This setup facilitated the acquisition of the infrared absorbance spectrum, enabling detailed analysis of the functional groups and chemical bonding present in the CNF/MFC and OP samples with different mechanical treatment durations.

Optical Microscopy

Optical microscopy was employed to investigate the morphological and size changes of OP and the corresponding chemically pretreated CNF/MFC under different durations of mechanical dispersing (0, 15, 30, 60, and 90 min). The images were taken at 10x and 50x magnifications to observe fibril micro- and nanostructures. The optical images were taken according to ISO 8576 (1996) by using an Olympus, model bx51, microscope (Olympus Corporation, Tokyo, Japan).

Cobb Test

The Cobb test was used to measure the water absorbency on the surface of paper and paperboard in this study, providing insights into the effectiveness of CNF/MFC coatings in improving the barrier properties of the base paper. This test is crucial for evaluating the hydrophobicity and water resistance of coated substrates, which is directly influenced by the coat weight, porosity, uniformity, and coverage of the applied CNF/MFC layer. The test was performed with a L&W Cobb sizing tester according to the ASTM D5795-16 (2024) standard (Lorentzon & Wettre, Stockholm, Sweden). The Cobb value (g/m²) was determined as the mass of water absorbed per unit area during a 60 s contact time. The Cobb test was repeated three times for each sample.

PPS Roughness

PPS roughness measures the surface roughness of paper under high pressure (1 MPa). A rotating metal head contacts the paper under pressure, and air leakage between the surface and the head is measured — the more air leakage, the rougher the surface. The coated papers were located under the nip and the selected pressure was applied on it. Each sample (CNF/MFC with different coating weights (1.5 to 3.7 g/m²)) was tested four times at different areas of the sample. These values evaluate how smooth the paper will be under nip pressure. PPS roughness was evaluated according to ISO 8791-3 (2017) using a PPS roughness tester (Parker Print-Surf Model M590, Messmer Büchel, Hoofddorp, the Netherlands)

Bendtsen Roughness

Bendtsen roughness measures the same parameter as PPS roughness, but with different mechanism and method. This test estimates surface roughness based on air leakage at low pressure (usually with a pressure of 1.47 kPa). Air is passed through a test head in contact with the coated papers with CNF/MFC that the more air passes, the rougher the surface. Bendtsen roughness was measured according to SS-ISO 8791-2 (2013) using a Bendtsen smoothness/roughness tester (Lorentzon & Wettre, Stockholm, Sweden).

Gurley Permeance

The Gurley permeance test is a critical measure of air resistance in the coated substrates, providing insight into the porosity and barrier performance of CNF/MFC coatings. A PPS tester (Parker Print-Surf Model M590, Messmer Büchel, Hoofddorp, the Netherlands) was used for the Gurley permeance test. This test was performed according to ISO 5636-5 (2013) and quantifies the time required for a specific volume of air (100 mL) to pass through a defined area of the coated papers with CNF/MFC as the samples under standardized pressure. Higher Gurley values indicate lower air permeability, reflecting a tighter, denser, and more uniform coating structure.

Bendtsen Permeance

Bendtsen permeance measures the air permeability of the coated papers with CNF/MFC, providing insights into the surface structure, porosity, and overall compactness of the coating layer. Unlike the Gurley test, which focuses on the time required for a fixed volume of air to pass through the sample, the Bendtsen test measures the volume of air flowing through a sample per unit time under a specified pressure (1.47 kPa). Bendtsen permeance was measured according to ISO 5636-3 (2013) using a Bendtsen smoothness/roughness tester (Lorentzon & Wettre, Stockholm, Sweden).

Surface Charge Measurements

Surface charge measurements of the materials were performed using a streaming current (SC) detector test, in order to determine the surface charge characteristics of cellulose nano/microfibrils (CNF/MFC) and original pulp (OP) samples in different mechanical treatment durations (0 and 90 min), which directly affect their colloidal stability and interaction with substrates. The test was performed according to SS-EN 22553-8 (2021) using a Mütek PCD-Titrator (BTG Instruments GmbH, Webling, Germany). The samples were diluted (0.01 to 0.05 wt.%) and were mixed with known amounts of cationic polymer poly-DADMAC (poly diallyl dimethylammonium chloride) with a charged group concentration of 0.001 N. The suspension of each sample with poly-DADMAC were stirred for 30 min to ensure complete binding of cationic charges to the negatively charged fibrils. After adsorption, the CNF/MFC was removed via vacuumfiltration to ensure only unbound poly-DADMAC remains in solution and to get the amount of CNF/MFC used in each sample. Filtrates were titrated with an anionic titrant sodium polyethylene sulfonate (NaPES) with a concentration of 0.001 N. The difference in polyelectrolyte volume before and after titration represents the net anionic surface charge. The analysis is based on an assumption that the cationic polymer had stoichiometrically complexed with accessible anionic groups on the CNF/MFC.

Drainage Resistance

Drainage resistance by the Schopper-Riegler test measures the rate at which water drains from a pulp suspension. The drainage resistance (°SR) was measured for the pulps. After Fenton reaction at 0, 15, 30, 60, and 90 min of mechanical treatment, all samples were tested in duplicate according to ISO 5267-1 (1999). The drainage testing was performed using a Schopper-Riegler apparatus (FRANK-PTI, Laakirchen, Austria).

RESULTS AND DISCUSSION

Structure and Properties of CNF/MFC

The FTIR spectra of the four samples, OP 0 min (original pulp, no chemical or mechanical treatment), OP 90 min (original pulp, 90 min mechanical dispersing), CNF/MFC 0 min (Fenton-oxidized cellulose, no mechanical dispersing), and CNF/MFC 90 min (Fenton-oxidized followed by 90 min mechanical dispersing) were recorded and analyzed to characterize chemical changes resulting from Fenton oxidation and subsequent mechanical fibrillation (see Fig. 4).

The overall FTIR spectrum is shown in Fig. 4 (a), which shows results corresponding to CNF/MFC and OP with either 0 or 90 min of mechanical treatment. This spectrum is then divided into two other spectra, shown in Fig. 4 (b) and (c). These spectral regions provide information regarding the produced samples in this study the O–H stretching envelope (3600 to 3000 cm⁻¹), the C–H stretching region (approximately 2940 to 2850 cm⁻¹), the water bending band (approximately 1645 to 1600 cm⁻¹), the crystallinity-sensitive CH₂ scissoring band (at about 1370-1430 cm⁻¹) and the fingerprint region (1160 to 1000 cm⁻¹) (Shanmugarajah *et al.* 2015).

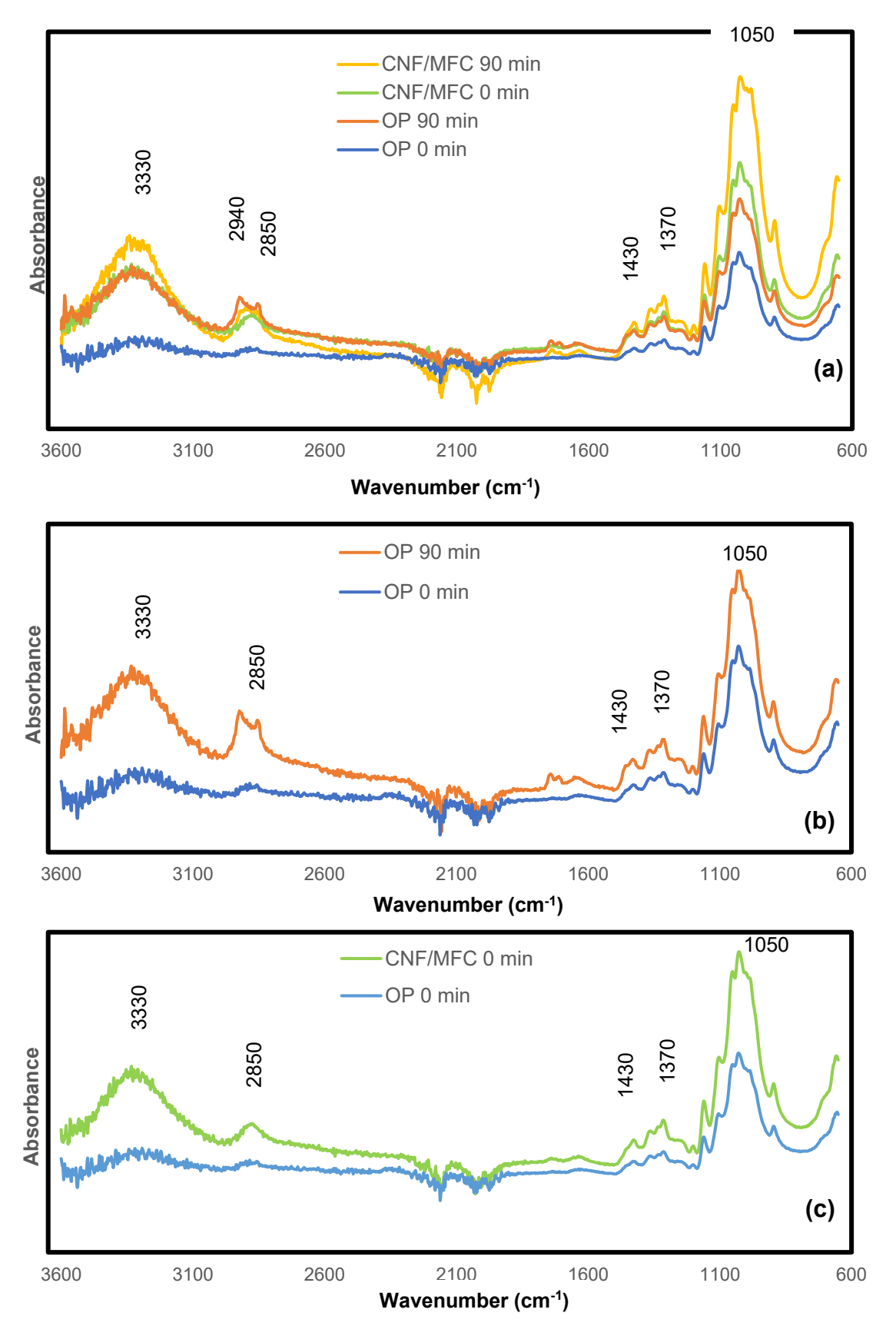


Fig. 4. (a) FTIR spectra of all samples, OP and CNF/MFC samples with 0 and 90 min dispersing. **(b)** FTIR spectra of only OP in 0 and 90 min **(c)** FTIR spectra of only OP and CNF/MFC in 0 min.

OP 0 min showed a moderate, broad O–H stretching envelope centered in the 3600 to 3000 cm⁻¹ region, clear but moderate C–H stretching intensity near 2940 to 2850 (cm⁻¹), a detectable H–O–H bending band around 1640 cm⁻¹ (indicative of physically adsorbed water), and identifiable fingerprint peaks in 1160 to 1050 (cm⁻¹) (Vijay *et al.* 2022; Menezes *et al.* 2021). The CH₂ scissoring band at about 1430 cm⁻¹ is distinguishable and typical for cellulose I, indicating the presence of ordered crystalline domains in the unprocessed pulp (C.S *et al.* 2016). These features are consistent with intact macroscopic fibers and limited exposed surface area. Microscopically, OP 0 min images show long, intact fibers and compact bundles (Fig. 5); the FTIR signature therefore reflects bulk cellulose with fewer externally accessible hydroxyl groups (Nagarajan *et al.* 2019; Mondragon *et al.* 2014).

As it is shown in Fig. 4 (b), after 90 min mechanical dispersing, OP 90 min shows systematic increases in the apparent absorbance of the O–H envelope and the fingerprint peaks (1160 to 1030 cm⁻¹). The C–H stretch also becomes slightly more pronounced. The H–O–H bending band (approximately 1640 cm⁻¹) remains present or shows a modest increase, indicating continued retention of bound water in the dispersed fragments. The CH₂ scissoring band near 1430 (cm⁻¹) shows a small change in shape/intensity that is consistent with the release of crystalline fragments but not with a wholesale loss of crystallinity (Li *et al.* 2018; Xu *et al.* 2021). These FTIR changes indicate that mechanical dispersing of untreated OP primarily liberates finer, more exposed cellulose surfaces (increasing the FTIR response of surface- and backbone-related vibrations) while preserving the cellulose I backbone chemistry (Nie *et al.* 2018). Optical micrographs (Fig. 5) for OP 90 min show partially frayed fibers and increased fines, which supports the FTIR evidence for increased surface exposure and orientation of cellulose chains (C.S *et al.* 2016; Nie *et al.* 2018).

The CNF/MFC 0 min sample (chemical pretreatment only) demonstrates distinct chemical changes relative to OP 0 min (Fig. 4 (c)). The O–H envelope is stronger and somewhat broader than OP 0 min, indicating increased polarity and a larger population of accessible hydroxyls produced by the oxidation step. The fingerprint peaks (1160 to 1050 cm⁻¹) are preserved and often clearer than OP 0 min (Menezes *et al.* 2021; Li *et al.* 2018). The carbonyl band (approximately 1735 cm⁻¹) is either absent or only visible as a weak shoulder, indicating that Fenton oxidation under the conditions used introduces limited amounts of discrete carbonyl/carboxyl groups sufficient to increase polarity and facilitate fibrillation but not to create heavy chemical modification or backbone cleavage (Li *et al.* 2018). The H–O–H bending band near 1640 cm⁻¹ is present and often comparable to OP 0 min, consistent with water adsorbed to oxidized fiber surfaces (Ruelas *et al.* 2023; Abraham *et al.* 2013). Microscopically CNF/MFC 0 min appears as weakened and more open fiber bundles (compared to OP 0 min), FTIR confirms that chemical pretreatment increases surface functionality without destroying the cellulose backbone (Liu *et al.* 2017).

CNF/MFC 90 min exhibits the most pronounced FTIR changes. The O–H stretching envelope (3600 to 3000 cm⁻¹) is strongest for this sample, indicating the greatest exposure of hydroxyl groups and highest surface polarity. Fingerprint bands in the 1160 to 1030 cm⁻¹ region are intensified and better resolved, while the CH₂ scissoring band at around 1430 cm⁻¹ is slightly reduced or broadened evidence of partial disruption of ordered crystalline lamellae as fibril layers are peeled apart. The 2000 to 2200 (cm⁻¹) window shows a deeper trough for CNF/MFC 90 min relative to the other samples (Li *et al.* 2018). This effect is interpreted as increased baseline modulation and scattering arising from a high concentration of nanoscale fibrils rather than the formation of new chemical

functionalities (Li et al. 2018; Menezes et al. 2021). Overall, the FTIR spectrum of CNF/MFC 90 min indicates mechanical peeling of oxidized fibers into a highly dispersed nano/microfibrillar network while the glycosidic backbone remains preserved. This chemical picture is borne out by optical microscopy; the CNF/MFC 90 min micrographs show a dense network of fine fibrils with few intact macrofibres, consistent with the enhanced surface-sensitive FTIR bands (Solfa et al. 2016; Nie et al. 2018).

Optical microscopy images of the original pulp and CNF/MFC samples at magnifications of $\times 10$ and $\times 50$ are presented in Fig. 5. Because microscopy is inherently qualitative, observations are limited to the fibers visualized, and no definitive conclusions can be drawn regarding the entire fiber population. The OP0 sample (original sample with no mechanical treatment) shows thick, rigid fibers with well-defined structures. These fibers are 10 to 20 μ m in diameter and 300 to 600 μ m in length. The fibrils in OP0 are largely intact, with almost no defibrillation. For CNF/MFC0, despite no mechanical dispersing (initially with 100 to 200 μ m length and 3 to 6 μ m diameter), some initial defibrillation is observed. This can be attributed to the Fenton oxidation treatment, which weakens the fiber wall structure. Fibers appear thinner and more swollen compared to the untreated OP0 sample.

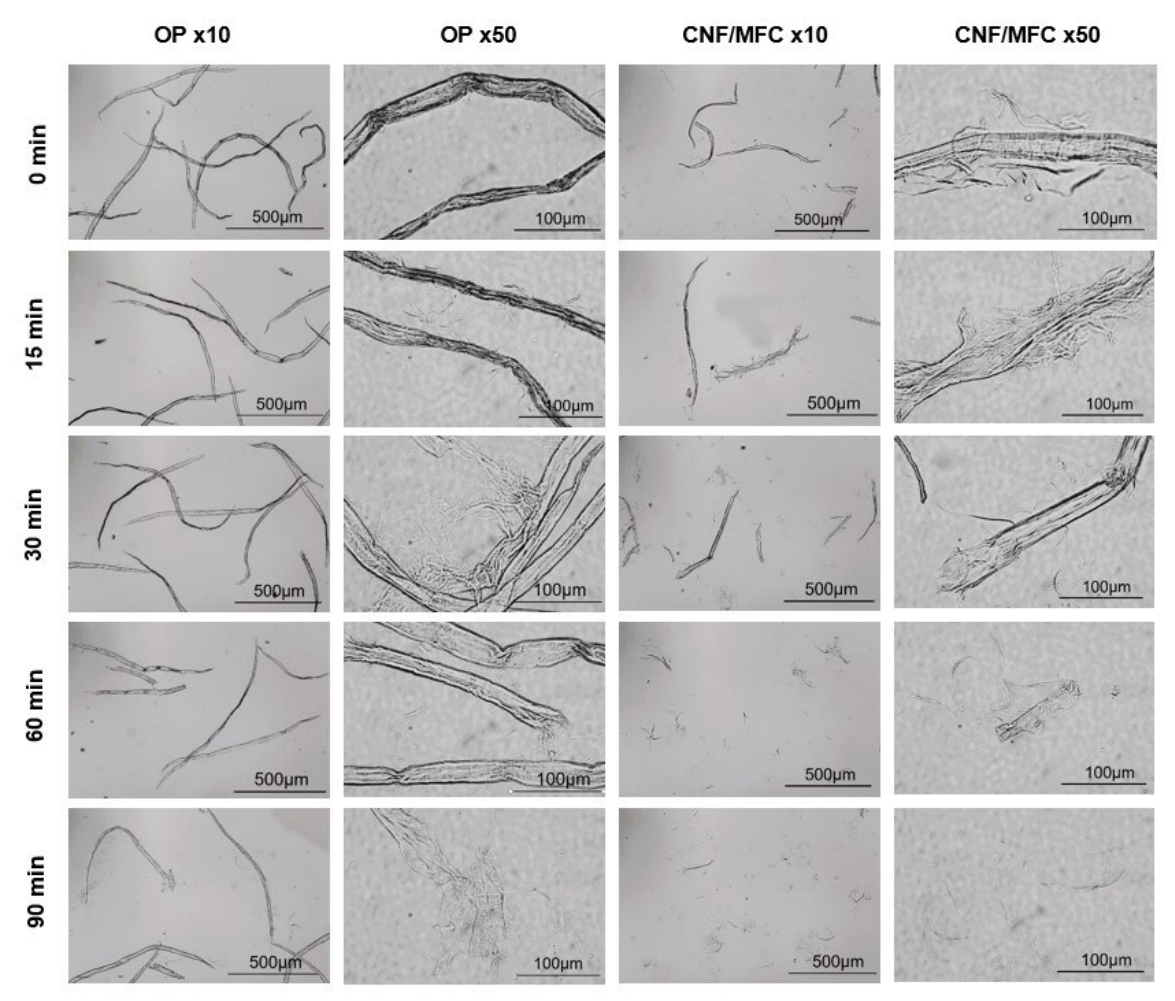


Fig. 5. Optical microscopic pictures for OP and CNF/MFC samples at magnifications x10 and x50 indicated by dispersing duration from 0 to 90 min

At 15 min of mechanical treatment, in OP15 sample, partial delamination of fibers is visible; bundles begin to split, forming smaller fines. The sizes of the OP15 sample are not changed significantly (300 to 400 μm length and 5 to 15 μm). In CNF/MFC15 a significant difference is visible compared to OP that the fibers are finer, with many short fibrils appearing (50 to 150 μm length and 1 to 3 μm diameter).

At 30 min in OP30, the fibers appear more fragmented. The diameter decreases slightly (3 to 6 μ m), and the individual fibrils become more distinguishable (100 to 300 μ m length). This shows that shear forces are effective in disrupting inter-fiber hydrogen bonds, initiating fibrillation (Li *et al.* 2014; Chandra *et al.* 2016). On the other side for CNF/MFC30, a clear increase in individualized fibrils is evident. The fiber network appears loosely entangled, with numerous short (20 to 100 μ m length) and thinner fibrils (0.5 to 2 μ m diameter), dispersed throughout the medium.

This demonstrates that chemical pretreatment (Fenton oxidation) greatly enhances fibrillation efficiency (Kiwi *et al.* 2002; Solfa *et al.* 2016). At 60 min, in the OP60 sample, an increased delamination is observed which is showing that fibers are more fibrillated than at 30 min. The average diameter of visible fibrils (2 to 5 μ m) further decreases, and fibers appear more elongated.

The images suggest that fibrils are undergoing longitudinal splitting (100 to 250 μm length), resulting in a higher aspect ratio. At the same dispersing duration, the CNF/MFC60 sample shows a high degree of fibrillation. Very fine fibrils, possibly in the nanometer range, dominate the image. Fibril bundles are highly reduced or absent, and the dispersing becomes more homogeneous. The reduction in both fiber length and diameter (10 to 50 μm length and 0.2 to 1 μm) indicates an effective breakdown of the fiber structure into smaller fibrils.

After prolonged mechanical treatment to 90 min, the OP90 appears highly fragmented (50 to 150 μ m) (Li *et al.* 2014; Nobuta *et al.* 2016). Very fine fibrillar structures are observed at higher magnification, though the optical resolution limits exact diameter measurement (1 to 2 μ m). Overall, the fiber network becomes denser and more entangled, indicating extensive fibrillation and possible formation of nanofibrils (Torlopov *et al.* 2019). At the same dispersing duration, the CNF/MFC60 sample shows a high degree of fibrillation. Very fine fibrils dominate the image. Fiber bundles are highly reduced or absent, and the dispersion becomes more homogeneous. The reduction in both fiber length and diameter (<20 μ m length and <0.1 μ m) indicates an effective breakdown of the cellulose structure into nano-sized fibrils (Li *et al.* 2018). Although optical microscopy is a visual method, Fig. 5 shows a clear effect of both mechanical and chemical treatments, with a significant difference between the original pulp (OP0) and the Fenton oxidized CNF/MFC samples.

Relation in Structure and Characteristics of CNF/MFC

The surface charge values indicate the amount of anionic surface charges associated with the fiber or fibril material. The surface charge influences interactions with additives, water retention, and dispersion stability (Nobuta *et al.* 2016), as shown in Table 2.

The CNF/MFC samples exhibit much higher anionic surface charge values than their OP counterparts, even without mechanical dispersing (CNF/MFC0: $67\pm4.0~\mu eq/g$ vs. OP0: $7.4\pm2.0~\mu eq/g$). This difference is primarily due to the smaller diameter and higher surface area of CNF/MFCs, which provide more accessible sites for carboxylation during Fenton oxidation.

Table 2. Surface Charge Results for CNF/MFC and OP Samples with Dispersing Times (0 and 90 min Mechanical Treatment)

Sample	Average of Surface Charge Results (µeq/g of cellulose material)	
CNF/MFC 90	90±4.4	
CNF/MFC 0	67±4.0	
OP 90	15±0.2	
OP 0	7.4±2.0	

The significant increase in charge density from 66±4.0 μeq/g (CNF/MFC0) to 90±4.4 μeq/g (CNF/MFC90) demonstrates that prolonged mechanical dispersing enhances the exposure of negatively charged carboxyl groups, introduced during the Fenton oxidation process (Solfa et al. 2016; Nagarajan et al. 2019). This 34% increase in charge density reflects a more extensive fibrillation process, which reduces fiber diameter and exposes a greater surface area, allowing more carboxyl groups to interact with the surrounding medium. Similarly, the original pulp samples show a notable increase from 7.4±2.0 μeq/g (OP0) to 15±0.2 μeq/g (OP90), representing a more than 100% increase in charge density. However, the absolute values remain significantly lower than the CNF/MFC samples, indicating that the pulp fibers, despite being oxidized, do not fibrillate as effectively as the nanoscale CNF/MFCs under similar mechanical treatment (Li et al. 2014; Vijay et al. 2022). The difference between CNF/MFC0 and CNF/MFC90 (23 μeg/g) is larger than the difference between OP0 and OP90 (8.0 µeq/g), indicating that CNF/MFCs benefit more from prolonged dispersing in terms of charge density enhancement, due to dispersing. The significantly higher surface charge in CNF/MFC90 (90 µeq/g) suggests superior electrostatic interaction potential, making this sample ideal for forming strong, uniform suspension (Dilamian et al. 2019; Menezes et al. 2021).

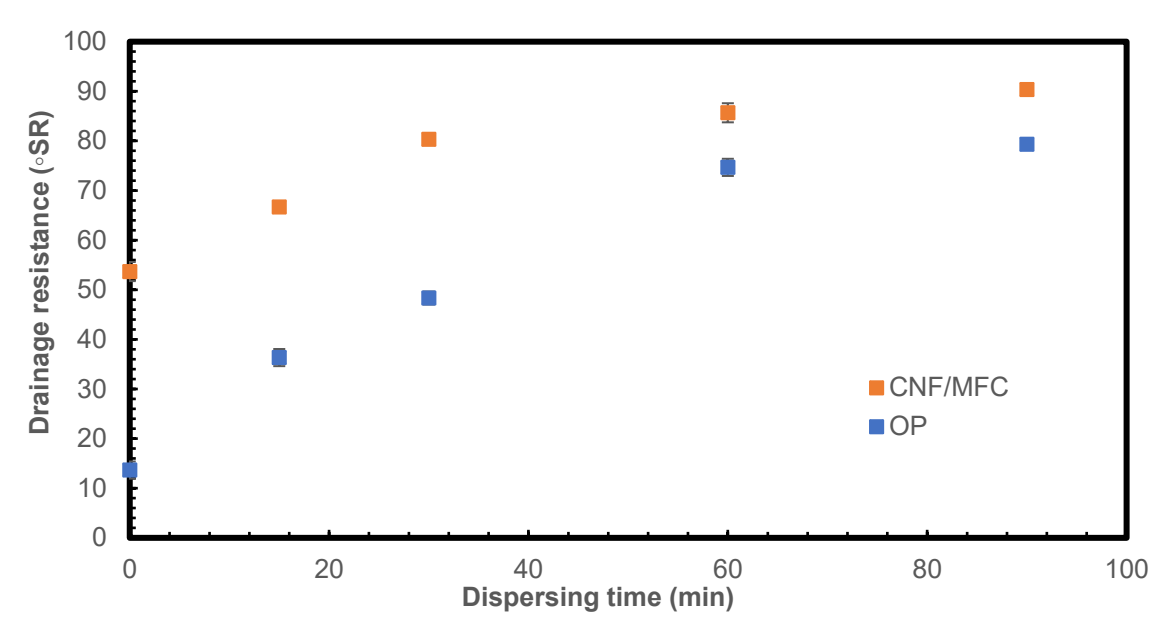


Fig. 6. Drainage resistance values (°SR) for CNF/MFC and OP samples at different dispersing times of 0 to 90 min

Mean drainage resistance values (°SR) were recorded with 95% confidence intervals, normally distributed, based on three repetitions at 0, 15, 30, 60, and 90 min dispersing times for the OP and CNF/MFC samples, as shown in Fig 6.

Water drainage decreased with dispersing time for both samples, indicating that fibrillation increased with mechanical treatment. CNF/MFC consistently showed higher SR values than OP due to chemical pretreatment in CNF/MFC that breaks down and weakens fiber walls (Ma et al. 2019). More extensive fibrillation increases the surface area and introduces a higher number of charged groups, which leads to slower drainage. This results in higher SR values, particularly in CNF/MFC samples subjected to chemical treatment, where the individualized fibrils form a denser network that retains water more effectively. OP showed a steady increase in drainage resistance, reflecting the gradual mechanical defibrillation. Formation of microfibrils and partially liberated fibers even at 90 min, OP retained some non-fibrillated or bundled fibers, which held more water. The plateau after 60 min (especially for CNF/MFC) showed near-complete fibrillation by this particular dispersing method, as shown by a level-off in the SR drainage resistance values (Feng et al. 2018; Li et al. 2018).

Barrier Coating on Paper Using CNF/MFC

For all coated samples, the coat weights ranging between 1.5 and 3.7 g/m², it is suspected that full coverage of the base paper was not achieved, even though the surface coverage ratio was not quantified in this work.

Fillat *et al.* (2023) evaluated one, five and ten layers of CNF to yield theoretical coating weights of 1, 5 and 10 g/m² and found that certain CNF types achieved good surface coverage even at lower coat weights. They showed that the coat weight required to obtain a continuous or nearly continuous CNF film varied depending on fibril morphology, coating method, and substrate porosity. The CNF coatings in the present work had similar basis weights and were thus expected to have a semi-continuous coverage.

In another study by Afra *et al.* (2016), base papers were coated with cellulose nanofibrils (CNF) at 1.5 wt% and 3 wt% concentrations, applied as single or double layers. The resulting coat weights were 2.3 g/m² (single 1.5 wt%), 4.1 g/m² (double 1.5 wt%), 3.0 g/m² (single 3 wt%), and 5.0 g/m² (double 3 wt%). Despite having the same total CNF content, the double 1.5 wt% coating produced a slightly higher coat weight and thicker layer than the single 3 wt% coating, due to better CNF penetration and distribution. SEM images showed that increased coating weight reduced surface porosity and improved uniformity. Consequently, higher coat weights and better coverage enhanced air resistance, surface smoothness, tensile strength, and barrier properties, while reducing water absorption and roughness.

In the present work, a single CNF layer formed a range of semi-continuous films, which were assumed to work as a coating enhancing paper properties although not completely covering the base paper.

The Cobb test results from the coated paper samples are shown in Fig. 7, covering a range of coat weights from 1.5 to 3.7 g/m 2 . The red square represents the reference Cobb value (39±3.3 g/m 2), for the uncoated paper.

The data show a non-linear relationship between coat weight and Cobb values, with a slight peak around 2.0 to 3.0 g/m², followed by a decrease at higher coat weights. Higher values indicate that the material is more hydrophilic, promoting greater water uptake and resulting in reduced water barrier performance. This increase is possibly due to the incomplete coverage of the paper fibers, resulting in uneven coating layers with exposed cellulose sites that remain highly hydrophilic (Li *et al.* 2018; Ruelas *et al.* 2023).

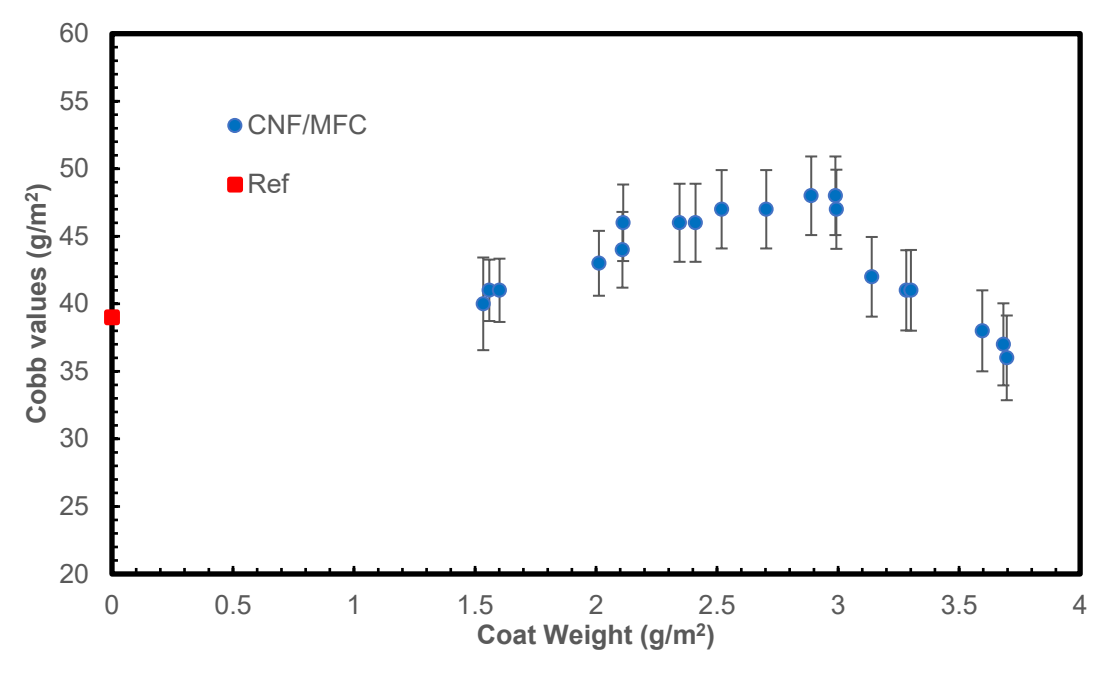


Fig. 7. Cobb test results for CNF/MFC coating and base paper as reference, indicated by the red square

At this stage, the CNF/MFC layer cannot yet act as a resistant enough film to act as an effective water barrier, allowing water to penetrate the underlying paper structure (Jonoobi *et al.* 2011). After the peak (about 3.0 g/m²), the Cobb value started to decline significantly as the coat weight increased, eventually dropping below the reference around 3.5 to 3.7 g/m². This decline indicates the formation of a more uniform, continuous, and denser CNF/MFC coating, starting to reduce the porosity of the paper and slightly enhancing its water resistance (Li *et al.* 2018; Xu *et al.* 2021). The point at which Cobb values fell below the reference line suggests a critical coat weight beyond which the CNF/MFC layer fully covered the paper surface, decreasing water absorption. In this particular case, coat weights more than 3.5 g/m² were needed to slightly increase the water barrier of the base paper.

There was a clear, positive relation between increasing coat weight and Gurley permeance (Fig. 8) with values rising from around 60 s to nearly 160 s as the coat weight increases, indicating a more closed sheet as the coat weight increases. The red square represents the baseline Gurley permeance for the uncoated or reference paper, set at 45 s, providing a benchmark for evaluating the effectiveness of the CNF/MFC coatings. At low coat weights (1.5 to 2.0 g/m²), the Gurley permeance values increase, but not very significantly, reflecting the initial formation of a thin CNF/MFC barrier that begins to restrict air flow (Potulski et al. 2020; Li et al. 2022). This likely corresponds to a partial surface coverage, where individual fibrils start to bridge the larger pores in the paper, creating a more tortuous path for air but not yet fully sealing the substrate. By increasing the coat weight from 2.0 to about 3.0 (g/m²), the Gurley values show a steep, consistent rise, indicating a more substantial reduction in air permeability, consistent with the behavior observed in the Cobb results (Fig. 8). This marks the transition to a denser, more continuous CNF/MFC coating, where the fibrils effectively block airflow by filling smaller pores and creating a tight, nanocellulose-rich surface layer (Zhu et al. 2011; Nie et al. 2018). The rise beyond 3.0 g/m² coat weights, suggests a critical threshold where the coating is dense enough to significantly limit air passage, a critical feature for applications requiring high barrier performance (Li et al. 2014; Nobuta et al. 2016).

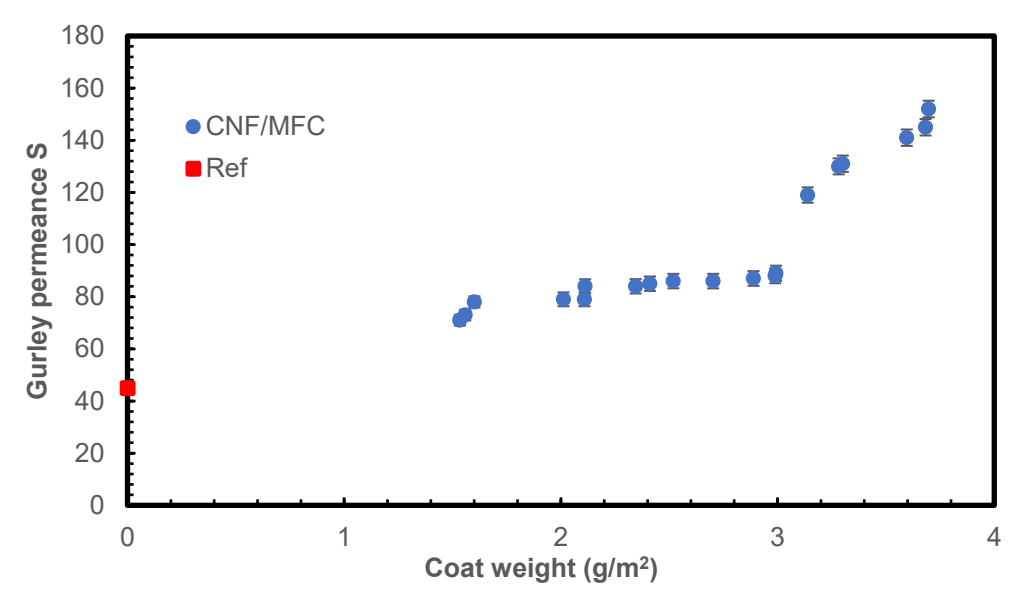


Fig. 8. Gurley permeance of CNF/MFC coating on paper, indicated as Ref by the red square

Bendtsen permeance test was done according to a range of coat weights (1.5 to 3.7 g/m²), and the results are shown in Fig. 9. At lower coat weights (1.5 to 2.0 g/m²), the permeance decreased from approximately 37 mL/min to around 30 mL/min. This initial drop corresponds to the early formation of a partial CNF/MFC network that began to seal the larger surface pores in the paper, reducing air flow but not yet achieving full coverage (Duan *et al.* 2020; Menezes *et al.* 2021).

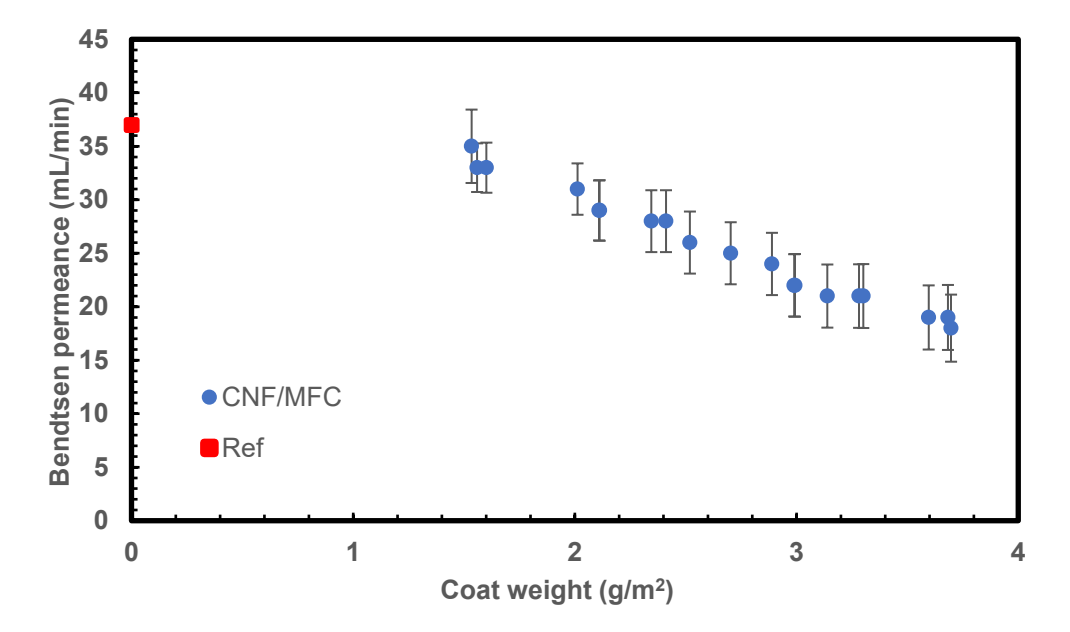
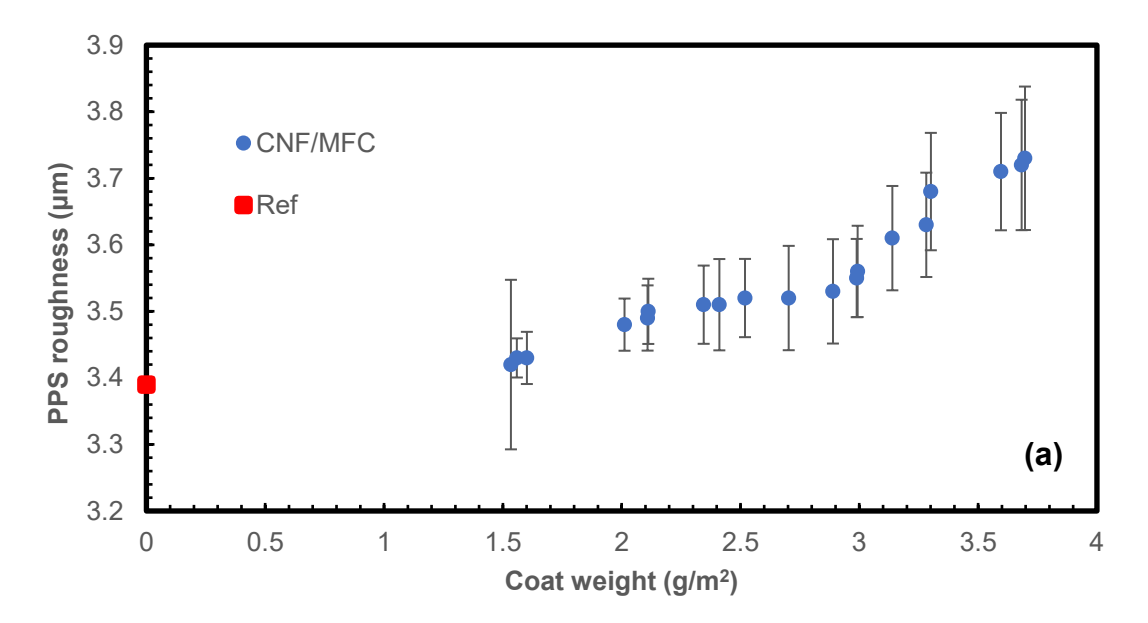


Fig. 9. Bendtsen permeance for CNF/MFC coating on paper, indicated as Ref by the red square

As the coat weight increased beyond 2.0 g/m², the permeance continued to decrease more gradually, reflecting the progressive densification of the CNF/MFC layer. The decline became more pronounced around 3.0 g/m², where the permeance dropped to below 20 mL/min, indicating a highly dense, low-porosity coating that effectively blocks air passage (Mondragon *et al.* 2014; Li *et al.* 2014). This region represents the point at which the CNF/MFC layer formed a continuous coherent coating, significantly reducing the number of air pathways through the substrate (Duan *et al.* 2020; Li *et al.* 2018). At the highest coat weights (3.5 to 3.7 g/m²), the permeance reached around 18 mL/min, suggesting a significant surface sealing effect at low coat weights.



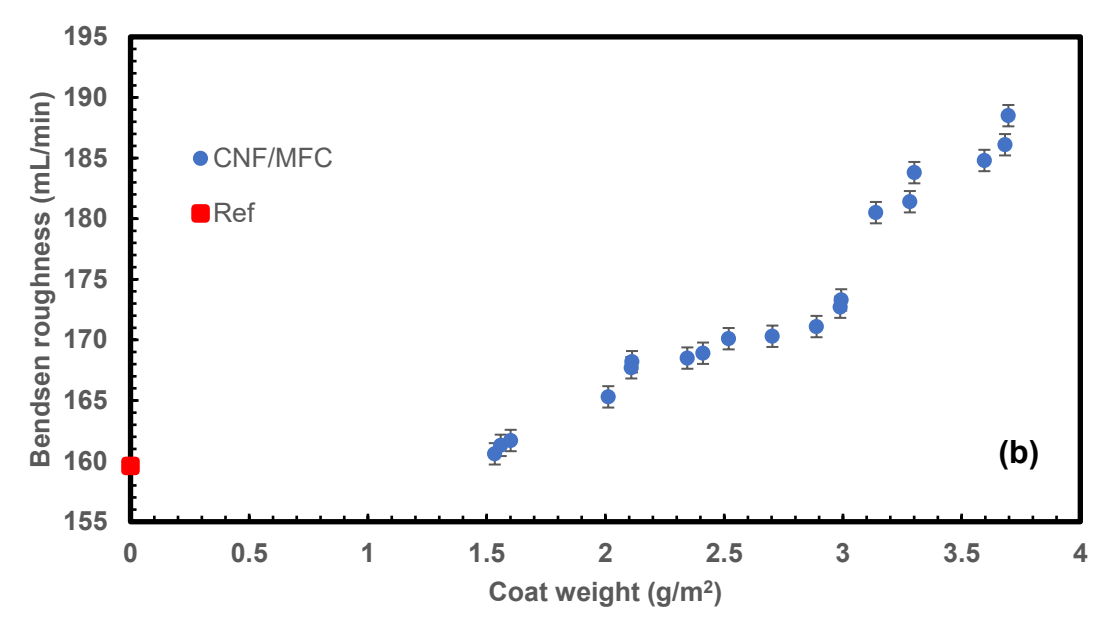


Fig. 10. The roughness results from (a) PPS test and (b) Bendtsen test for CNF/MFC coating on paper, indicating Ref as red square

A roughness technique was applied on CNF/MFC and paper-based substance with PPS roughness tester. As the coat weight increases from 1.5 to 3.7 g/m², the PPS roughness rose steadily (see Fig. 10 (a)). This upward trend indicates that higher CNF/MFC coat weights resulted in rougher surfaces due to increased fiber network formation and surface irregularities at higher application levels. Notably, this relationship appeared to be nonlinear, with the roughness increment becoming more pronounced beyond 3 g/m². This suggests a threshold after which the densification effect of the CNF/MFC matrix began to dominate, possibly due to enhanced fiber entanglement and reduced pore collapse resistance. Notably, Bendtsen roughness trend aligns with the PPS roughness results, suggesting that the structural characteristics driving surface irregularities are consistent across different measurement methods (Li *et al.* 2011; Abraham *et al.* 2013; Chandra *et al.* 2016).

Another roughness test was applied on CNF/MFC coated papers with Bendtsen roughness tester, and these results are shown in Fig. 10 (b). At lower coat weights (1.5 to 1.6 g/m²), the roughness remained relatively close to the baseline reference level of around 160 mL/min, suggesting that the initial CNF/MFC layers effectively fill smaller surface voids, leading to a more uniform overall structure. As the coat weight increased beyond 2.0 g/m², the roughness began to steady rise, reflecting the formation of a thicker, potentially more fibrous and less densely packed CNF/MFC layer (Potulski *et al.* 2020; Vijay *et al.* 2024). This trend continued up to approximately 3.7 g/m², where the roughness was near 190 mL/min. This increase in roughness at higher coat weights can be attributed to the inherent nanofibrillar structure of the CNF/MFC, which, while capable of filling micro-scale pores, may introduce additional surface irregularities as the coating thickness (Dilamian *et al.* 2019).

The air permeance and roughness results indicate that the coatings were relatively low in density, unlike TEMPO-oxidized CNF, which typically forms dense barrier layers. This difference is likely due to the Fenton oxidation combined with mechanical dispersing, producing well-fibrillated particles that do not pack as tightly, resulting in a more open, porous network with higher roughness and air permeability (Gamelas *et al.* 2015; Ammala *et al.* 2022).

CONCLUSIONS

- 1. Cellulose nanofibril/microfibrillated cellulose (CNF/MFC) products were successfully produced from hardwood pulp *via* Fenton oxidation followed by mechanical dispersion enhancing fiber fibrillation to form nanoscale and microscale structures.
- 2. Fourier transform infrared (FTIR) spectrometry confirmed chemical modifications and introduction of carboxyl functionalities, while optical microscopy (×10 and ×50) verified fiber defibrillation over different dispersing durations.
- 3. Fenton oxidation (0 min) prepared fibers for mechanical delamination, and mechanical dispersing (90 min) increased accessible surface area, exposed backbone functional groups. The 90-minute treatment resulted in CNF/MFC with maximal O–H exposure, partial crystallinity reduction, and a visible nanoscale fibrillar network.
- 4. Drainage resistance measurements showed that CNF/MFC drained slower than the original bleached hardwood kraft pulp (OP), reaching a plateau at 60 min for nearly complete conversion into nano- and microfibrils, whereas OP achieved only partial

- fibrillation, consistent with microscopy. Physical tests (Cobb, Gurley, Bendtsen, PPS roughness and air permeance) indicated significant changes; highest coat weights produced an 85% reduction in air permeance and a minimum coat weight of roughly 3.0 g/m² was critical for barrier performance.
- 5. The surface charge analysis revealed increased surface charge, enhancing performance and interactions with additives or fillers. Overall, Fenton oxidation coupled with mechanical dispersion effectively produced CNF/MFC from hardwood pulp, yielding materials with pronounced chemical, morphological, and functional improvements suitable for various applications.

ACKNOWLEDGMENTS

The authors wish to express their sincere gratitude to Carl-Anton Karlsson for his invaluable assistance with the laboratory work and his expert guidance in the operation of laboratory instruments. Appreciation is also extended to Niklas Kvarnlöf of Billerud AB for generously providing the pulp utilized in this study, and to Gunilla Carlsson Kvarnlöf for discussion of the FTIR results during peer review.

REFERENCES CITED

- Abraham, E., Deepa, B., Pothen, L. A., Cintil, J., Thomas, S., Johan, M. J., Anandjiwala, R., and Narine, S. S. (2013). "Environmental friendly method for the extraction of coir fibre and isolation of nanofibre," *Carbohydrate Polymers* 92, 1477-1483. https://doi.org/10.1016/j.carbpol.2012.10.056
- Afra, E., Mohammadnejad, S., and Saraeyan, A. (2016). "Cellulose nanofibrils as coating material and its effects on paper properties," *Progress in Organic Coatings* 101, 455-460. https://doi.org/10.1016/j.porgcoat.2016.09.018
- Ammala, A., Sirvio, J. A., Liimatainen, H. (2022). "Pine sawdust modification using Fenton oxidation for enhanced production of high-yield lignin-containing microfibrillated cellulose," *Industrial Crops & Products* 186, article 115196. https://doi.org/10.1016/j.indcrop.2022.115196
- ASTM (2024). "Standard test method for water absorption of paperboard (Cobb test)," ASTM D5795-16, ASTM International, West Conshohocken, PA, USA.
- Bahrami, B., Behzad, T., Zamani, A., Heidarian, P., and Nasrabadi, B. N. (2018). "Optimal design of ozone bleaching parameters to approach cellulose nanofibers extraction from sugarcane bagasse fibers," *Polymers and the Environment* 26, 4085-4094. https://doi.org/10.1007/s10924-018-1277-5
- Bautista, P., Mohedano, F. A., Casas, A. J., Zazo, A. J., and Rodriguez, J. J. (2008). "An overview of the application of Fenton oxidation to industrial wastewaters treatment," *Chemical Technology and Biotechnology* 83, 1323-1338. https://doi.org/0.1002/jctb.1988
- Boufi, S., Gonzalez, I., Aguilar, D. M., Tarres, Q., Pelach, A. M., and Mutje, P. (2016). "Nanofibrillated cellulose as an additive in papermaking process," *Carbohydrate Polymers* 154 (2016) 151-166. https://doi.org/10.1016/j.carbpol.2016.07.117 Chandra, J. C. S., George, N., and Narayanankutty, S. K. (2016). "Isolation and

- characterization of cellulose nanofibrils from arecanut husk fibre," *Carbohydrate Polymers* 142, 158-166. https://doi.org/10.1016/j.carbpol.2016.01.015
- Correa, A. C., Teixeira, E., Pessan, L. A., and Mattoso, L. H. C. (2010). "Cellulose nanofibers from curaua fibers," *Cellulose* 17, 1183-1192. https://doi.org/10.1007/s10570-010-9453-3
- Dilamian, M., and Noroozi, B. (2019). "A combined homogenization-high intensity ultrasonication process for individualization of cellulose micro-nano fibers from rice straw," *Cellulose* 26, 5831-5849. https://doi.org/10.1007/s10570-019-02469-y
- Duan, L., Liu, R., and Li, Q. (2020). "A more efficient Fenton oxidation method with high shear mixing for the preparation of cellulose nanofibers," *Starch* 72, article 1900259. https://doi.org/10.1002/star.201900259
- Feng, Y. H., Cheng, T. Y., Yang, W. G., Ma, P. T., He, H. Z., Yin, X. C., and Yu, X. X. (2018). "Characteristics and environmentally friendly extraction of cellulose nanofibrils from sugarcane bagasse," *Industrial Crops and Products* 111, 285-291. https://doi.org/10.1016/j.indcrop.2017.10.041
- Fillat, U., Vergara, P., Villar, J. C., and Gomez, N. (2023). "Structural properties of coated papers with cellulosic nanofibres using different metering systems and drying technologies," *Progress in Organic Coatings* 179, article 107543. https://doi.org/10.1016/j.porgcoat.2023.107543
- Gamelas, J. A. F., Pedrosa, Jorge., Lourenco, A. F., Mutje, P., Gonzalez, I., Carrasco, G. C., Singh, G., and Ferreira, P. J. T. (2015). "On the morphology of cellulose nanofibrils obtained by TEMPO-mediated oxidation and mechanical treatment," *Micron* 72, 28-33. https://doi.org/10.1016/j.micron.2015.02.003
- Hellström, P., Hulten, A. H., Paulsson, M., Håkasson, H., and Germgård, U. (2014). "The effect of Fenton chemistry on the properties of microfibrillated cellulose," *Cellulose* 21, 1489-1503. https://doi.org/10.1007/s10570-014-0243-1
- ISO 20579-3 (2021). "Surface chemical analysis Electron spectroscopies Part 3: Reporting of methods used for charge control and charge correction," International Organization for Standardization, Geneva, Switzerland.
- ISO 5267-1 (1999). "Pulps Determination of drainability Part 1: Schopper-Riegler method," International Organization for Standardization, Geneva, Switzerland.
- ISO 5636-3 (2013). "Paper and board Determination of air permeance (medium range)
 Part 3: Bendtsen method," International Organization for Standardization, Geneva, Switzerland.
- ISO 5636-5 (2013). "Paper and board Determination of air permeance (medium range)
 Part 5: Gurley method," International Organization for Standardization, Geneva,
 Switzerland.
- ISO 8576 (1996). "Optical microscopy General requirements," International Organization for Standardization, Geneva, Switzerland.
- ISO 8791-3 (2017). "Paper and board Determination of roughness/smoothness (air leak methods) Part 3: PPS method," International Organization for Standardization, Geneva, Switzerland.
- Jonoobi, M., Khazaeian, A., Tahir, P. M., Azry, S. S., and Oksman, K. (2011). "Characteristics of cellulose nanofibers isolated from rubberwood and empty fruit bunches of oil palm using chemo-mechanical process," *Cellulose* 18, 1085-1095. https://doi.org/10.1007/s10570-011-9546-7
- Kiwi, J., Denisov, N., Ovanesyan, N., Buffat. P. A., Sucorova, E., Gostev, F., Titov, A., Sarkisov, O., Albers, P., and Nadtochenko, V. (2002). "Catalytic Fe³⁺ clusters and

- complexes in Nafion active in photo-Fenton processes. High-Resolution electron microscopy and femtosecond studies," *Langmuir* 18(23), 9054-9066. https://doi.org/10.1021/la020648k
- Li, J., Liu, D., Li, J., Yang, F., Sui, G., and Dong, Y. (2022). "Fabrication and properties of tree-branched cellulose nanofibers (CNFs) *via* acid hydrolysis assisted with predisintegration treatment," *Nanomaterials* 12(12), article 2089. https://doi.org/10.3390/nano12122089
- Li, M., Wang, L. J., Li, D., Cheng, Y. L., and Adhikari, B. (2014). "Preparation and characterization of cellulose nanofibers from de-pectinated sugar beet pulp," *Carbohydrate Polymers* 102, 136-143. https://doi.org/10.1016/j.carbpol.2013.11.021
- Li, Q., Wang, A., Long, K., He, Z., and Cha, R. (2018). "Modified Fenton oxidation of cellulose fibers for cellulose nanofibrils preparation," *ACS Sustainable Chemistry & Engineering* 7(1), 1129-1136. https://doi.org/10.1021/acssuschemeng.8b04786
- Liu, Q., Lu, Y., Aguedo, M., Jacquet, N., Ouyang, C., He, W., Yan, C., Bai, W., Guo, R., Goffin, D., Song, J., and Richel, A. (2017). "Isolation of high-purity cellulose nanofibers from wheat straw through the combined environmentally friendly methods of steam explosion, microwave-assisted hydrolysis, and microfluidization," *ACS Sustainable Chemistry & Engineering* 5, 6183-6191. https://doi.org/10.1021/acssuschemeng.7b01108
- Ma, Y., Xia, Q., Liu, Y., Chen, W., Liu, S., Wang, Q., Liu, Y., Li, J., and Yu, H. (2019). "Production of nanocellulose using hydrated deep eutectic solvent combined with ultrasonic treatment," *ACS Omega* 4, 8539-8547. https://doi.org/10.1021/acsomega.9b00519
- Menezes, D. B., Diz, F. M., Ferreira, L. F. R., Corrales, Y., Baudrit, J. R. V., Costa, L. P., and Hernandez-Macedo, M. L. (2021). "Starch-based biocomposite membrane reinforced by orange bagasse cellulose nanofibers extracted from ionic liquid treatment," *Cellulose* 28, 4137-4149. https://doi.org/10.1007/s10570-021-03814-w
- Mondragon, G., Fernandes, S., Retegi, A., Pena, C., Algar, I., Eceiza, A., and Arbelaiz, A. (2014). "A common strategy to extracting cellulose nanoentities from different plants," *Industrial Crops and Products* 55, 140-148. https://doi.org/10.1016/j.indcrop.2014.02.014
- Nagarajan, K. J., Balaji, A. N., and Ramanujan, N. R. (2019). "Extraction of cellulose nanofibers from *Cocos nucifera* var *aurantiaca* peduncle by ball milling combined with chemical treatment," *Carbohydrate Polymers* 212, 312-322. https://doi.org/10.1016/j.carbpol.2019.02.063
- Nie, S., Zhang, K., Lin, X., Zhang, C., Yan, D., Liang, H., and Wang, S. (2018). "Enzymatic pretreatment for the improvement of dispersion and film properties of cellulose nanofibrils," *Carbohydrate Polymers* 181, 1136-1142. https://doi.org/10.1016/j.carbpol.2017.11.020
- Nobuta, K., Teramura, H., Ito, H., Hongo, C., Kawaguchi, H., Ogino, C., Kondo, A., and Nishino, T. (2016). "Characterization of cellulose nanofiber sheets from different refining processes," *Cellulose* 23, 403-414. https://doi.org/10.1007/s10570-015-0792-y
- Paniz, O. G., Pereira, C. M. P., Pacheco, B. S., Wolke, S. I., Maron, G. K., Mansilla, A., Colepicolo, P., Orlandi, M. O., Osorio, A. G., and Carreno, N. L. V. (2020). "Cellulosic material obtained from Antarctic algae biomass," *Cellulose* 27, 113-126. https://doi.org/10.1007/s10570-019-02794-2
- Petroudy, S. R. D., Chabot, B., Loranger, E., Naebe, M., Shojaeiarani, J., Gharehkhani,

- S., Ahvazi, B., Hu, J., and Thomas, S. (2021). "Recent advances in cellulose nanofibers preparation through energy-efficient approaches," *Energies* 14, article 6792. https://doi.org/10.3390/en14206792
- Potulski, D. C., Viana, L. C., Fonte, A. N., Carneiro, M. E., Muniz, G. I. B., and Klock, U. (2020). "Nano fibrillated cellulose applied as reinforcement for short-fiber paper," Floresta 50(3), article 1411. https://doi.org/10.5380/rf.v50i3.59251
- Pouran, S. R., Aziz, A. R. A., and Daud, W. M. A. W. (2015). "Review on the main advances in photo-Fenton oxidation system for recalcitrant wastewaters," *Industrial and Engineering Chemistry* 21, 53-69. https://doi.org/10.1016/j.jiec.2014.05.005
- Ruelas, A. R. B., Vidal, Y. R., Campuzano, J. R. I., and Cuevas, L. R. (2023). "Simultaneous oxidation of emerging pollutants in real wastewater by the advanced Fenton oxidation process," *Catalysts* 13(4), article 748. https://doi.org/10.3390/catal13040748
- Shanmugarajah, B., Kiew, P. L., Chew, I. M. L., Choong, T. S. Y., Tan, K. W. (2015). "Isolation of nanocrystalline cellulose (NCC) from palm oil empty fruit bunch (EFB): Preliminary result on FTIR and DLS analysis," *Chemical Engineering Transactions* 45, 2283-9216. https://doi.org/10.3303/CET1545285
- Solfa, M. R. K., Brown, R. J., Tsuzuki, T., and Rainy, T. J. (2016). "A comparison of cellulose nanocrystals and cellulose nanofibres extracted from bagasse using acid and ball milling methods," *Advances in Natural Sciences: Nanoscience and Nanotechnology* 7, article 035004. https://doi.org/10.1088/2043-6262/7/3/035004
- SS-EN 22553-8 (2021). "Paper, board and pulps Determination of particle charge," Swedish Standards Institute, Stockholm, Sweden.
- SS-ISO 8791-2 (2013). "Paper and board Determination of roughness/smoothness (air leak methods) Part 2: Bendtsen method," Swedish Standards Institute, Stockholm, Sweden.
- Sulaiman, S., Mokhtar, M. N., Naim, M. N., Baharuddin, A. S., and Sulaiman, A. (2015). "Potential usage of cellulose nanofibers (CNF) for enzyme immobilization via covalent interactions," *Appl Biochem Biotechnol* 175, 1817-1842. https://doi.org/10.1007/s12010-014-1417-x
- Torlopov, M. A., Martakov, L. S., Mikhaylov, V. I., Golubev, Y. A., Sitnikov, P. A., and Udoratina, E. V. (2019). "A Fenton-like system (Cu (II)/H₂O₂) for the preparation of cellulose nanocrystals with a slightly modified surface," *ACS Sustainable Chemistry & Engineering* 58(44), 20282-20290. https://doi.org/10.1021/acs.iecr.9b03226
- Vijay, P., Batchelor, W., and Saito, K. (2022). "One-pot treatment of cellulose using iron oxide catalysts to produce nanocellulose and water-soluble oxidized cellulose," *Carbohydrate Polymers* 282, article 119060. https://doi.org/10.1016/j.carbpol.2021.119060
- Vijay, P., Raghuwanshi, S. V., Ma, J., Batchelor, W., and Saito, K. (2024). "Fenton-like oxidation of pinewood to produce cellulose nanoparticles in one pot treatment," *Cellulose* 31, 953-967. https://doi.org/10.1007/s10570-023-05573-2
- Xu, X., Lu, N., Wang, S., Huang, M., Qu, S., and Xuan, F. (2021). "Extraction and characterization of microfibrillated cellulose from discarded cotton fibers through catalyst preloaded Fenton oxidation," *Advances in Materials Science and Engineering* 2021(1), article 545409. https://doi.org/10.1155/2021/5545409

418

Zhu, X., Tian, J., Liu, R., and Chen, L. (2011). "Optimization of Fenton and electro-Fenton oxidation of biologically treated coking wastewater using response surface methodology," *Separation and Purification Technology* 81 (2011) 444-450. https://doi.org/10.1016/j.seppur.2011.08.023

Article submitted: September 5, 2025; Peer review completed: November 1, 2025; Revised version received and accepted: November 10, 2025; Published: November 19, 2025.

DOI: 10.15376/biores.21.1.397-419